# Comparison Between 2D and 3D Dosimetry Protocols in ^{90}Y-Ibritumomab Tiuxetan Radioimmunotherapy of Patients with Non-Hodgkin's Lymphoma

**Karine Assié,[1,2] Arnaud Dieudonné,[1] Isabelle Gardin,[1,3] Irène Buvat,[2] Hervé Tilly,[4] and Pierre Vera[1,3]**

[1]Laboratoire LITIS (EA 4108), Université de Rouen, Rouen, France
[2]Unité 678 INSERM – Université Pierre et Marie Curie, Centre Hospitalier Universitaire Pitié-Salpêtrière, Paris, France
[3]Département de Médecine Nucléaire, Centre Hospitalier Universitaire, Centre Henri Becquerel, Rouen, France
[4]Département d'Hématologie et Groupe d'Etude des Proliférations Lymphoïdes, INSERM U614, IFR23, Centre Henri Becquerel, Rouen, France

## ABSTRACT

*We compared the radiation-absorbed dose obtained from a two dimensional (2D) protocol, based on planar whole-body (WB) scans and fixed reference organ masses with dose estimates, using a 3D single-photon emission computed tomography (SPECT) imaging protocol and patient-specific organ masses. **Methods:** Six (6) patients with follicular non-Hodgkin's lymphoma underwent a computed tomography (CT) scan, 5 2D planar WB, and 5 SPECT scans between days 0 and 6 after the injection of ^{111}In-ibritumomab tiuxetan. The activity values in the liver, spleen, and kidneys were calculated from the 2D WB scans, and also from the 3D SPECT images reconstructed, using quantitative image processing. Absorbed doses after the administration of ^{90}Y-ibritumomab tiuxetan were calculated from the ^{111}In WB activity values combined with reference organ masses and also from the SPECT activity values and organ masses as estimated from the patient CT scan. To assess the quantitative accuracy of the WB and SPECT scans, an abdominal phantom was also studied. **Results:** The differences between organ masses estimated from the patient CT and from the reference MIRD models were between −10% and +98%. Using the phantom, errors in organ and tumor activity estimates were between −86% and 10% for the WB protocol and between −43% and −6% for the SPECT protocol. Patient liver, spleen, and kidney activity values determined from SPECT were systematically less than those from the WB scans. Radiation-absorbed doses calculated with the 3D protocol were systematically lower than those calculated from the WB protocol (29% ± 26%, 73% ± 26%, and 33% ± 53% differences in the liver, spleen, and kidney, respectively), except in the kidneys of 2 patients and in the liver of 1 patient. **Conclusions:** Accounting for patient-specific organ mass and using SPECT activity quantification have both a great impact on estimated absorbed doses.*

**Key words:** 3D dosimetry, radioimmunotherapy, ^{90}Y-ibritumomab tiuxetan

*Address reprint requests to: Isabelle Gardin; Nuclear Medicine Department, Centre Henri Becquerel; 1 rue d'Amiens, 76038 Cedex, Rouen, France; Tel.: +33-2-32-08-22-54; Fax: +33-2-32-08-25-50*
*E-mail: igardin@rouen.fnclcc.fr*

## INTRODUCTION

Radioimmunotherapy (RIT) with pure $\beta$-emitter-yttrium-90 ($^{90}$Y)-labeled antibodies permit the efficient delivery of ionizing radiation to targeted cells while limiting the radiation dose to normal nontargeted tissues. The $^{90}$Y-labeled antibody, $^{90}$Y-ibritumomab tiuxetan (ZEVALIN®; Schering AG, Berlin, Germany), is directed against the B-lymphocyte CD20 antigen. In a randomized, phase III trial comparing the efficacy of 15 MBq/kg $^{90}$Y ibritumomab tiuxetan with 4 weekly doses of rituximab in patients with relapsed or refractory low-grade, follicular, or transformed CD20$^+$ B-cell lymphoma, the overall response rate was significantly higher in the $^{90}$Y-ibritumomab tiuxetan group than in the rituximab group (80% vs. 56%; $p = 0.002$), and the complete response rate was almost twice as high in the RIT group (30% vs. 16%; $p = 0.04$).[1] $^{90}$Y-ibritumomab tiuxetan is the first radioimmunoconjugate that has been approved by the U.S. Food and Drug Administration and the European authorities for the treatment of patients with relapsed or refractory low-grade, follicular, or transformed B-cell non-Hodgkin's Lymphoma (NHL), including patients with rituximab-refractory follicular lymphoma.

As a pure $\beta$-emitter, $^{90}$Y has no $\gamma$-photon for biodistribution and dosimetry evaluations. Preclinical studies have demonstrated that the biodistribution of $^{90}$Y-ibritumomab tiuxetan is adequately predicted by the $^{111}$In-labeled (indium-111) antibody.[2,3] As $^{111}$In emits $\gamma$-rays and has a half-life duration (67.9 hours) comparable with that of $^{90}$Y (64.8 hours), the $^{111}$In-labeled agent is generally used as a chemical and biologic surrogate to trace the biodistribution of the $^{90}$Y-labeled therapeutic agent.[4]

Dosimetry studies are usually performed by using the well-established two-dimensional (2D) method proposed by the Medical Internal Radiation Dose (MIRD) Committee.[5,6] Wiseman et al. estimated the median and the range of the absorbed dose to spleen (7.42 Gy [0.76–24.5]), to liver (4.50 Gy [1.22–18.6]), and to kidneys (0.23 Gy [0–0.76]) after a therapeutic administration of $^{90}$Y-ibritumomab tiuxetan ($n = 129$ patients, 15 MBq/kg [maximum 1.2 GBq] administered).[7] The two main drawbacks of this 2D method are that whole-body (WB) scans do not easily lend themselves to accurate estimates of the activity distributions in organs,[8] and that the protocol does not take into account variations in organ mass seen within individual patients.[9] A 3D single-photon emission computed tomography (SPECT) imaging approach is better suited for accurate quantification of the activity distribution, since it allows for corrections for most detection phenomena that introduce quantitative biases in planar images, namely photon scatter, attenuation, and partial volume effect, as well as overlap between organs. Regarding organ masses, several researchers have demonstrated the wide variability in normal organ size,[9,10] which tend to be accentuated among diseased patients owing to edema, inflammation, and other pathologies. Since the absorbed dose to an organ is inversely proportional to its mass, an adjustment to the dose estimation should be made, given patient-specific information on organ masses. It has been proposed that dosimetry protocols properly adjust reference patient doses by using computed tomography (CT)-derived patient organ masses ($m_{CT}$).[10] Biases in activity quantification from planar imaging combined with the use of simple geometric representations of human organs can potentially lead to either gross under- or overestimates of the true radiation-absorbed dose to patient organs. The poor correlation between radiation-absorbed dose and tumor response or normal tissue toxicity observed, so far, in targeted radiotherapy might be owing, in part, to inaccuracies in the estimated absorbed dose due to either or both of these sources of error.[11–13]

Our goal was to assess the two main sources of error in radiation-absorbed dose computation, namely activity measurement and the use of standardized organ mass, when considering a 2D imaging protocol and fixed reference patient organ masses. This study related to liver, spleen, and kidney dose estimates in $^{90}$Y-ibritumomab tiuxetan targeted RIT. The accuracy of performing dose calculations from a 3D imaging protocol, considering actual organ mass derived from CT volumetry and activity measurements from quantitative SPECT imaging, was compared to that of a 2D approach. To objectively assess the accuracy of absolute activity measurements from 2D WB and SPECT scans, an abdominal physical phantom experiment was also performed.

## MATERIALS AND METHODS

### Imaging Phantom

A Liqui-Phil™ abdominal phantom (The Phantom Laboratory, New York, NY) was used, which contains six inserts simulating the liver, spleen,

right and left kidneys, and two spherical tumors of an inner radius equal to 40 and 20 mm. The smallest sphere was placed between the two kidneys, whereas the largest sphere was placed near the liver close to the center of the phantom. The volume of each insert and the associated $^{111}$In activity values corresponded to nominal activities expected in actual patients, as given in Table 1.

**Patient Population**

All 6 patients, 2 males and 4 females, with a mean age of 53 years (range, 38–66) included by the Centre Henri Becquerel (Rouen, France) in a European and Canadian phase III trial of $^{90}$Y-ibritumomab tiuxetan were considered for comparing the results of 2D and 3D calculations of the organ absorbed dose. The aim of the clinical trial was to study the efficacy and safety of treatment with ZEVALIN versus no further treatment in patients with stage III or IV follicular NHL having achieved partial or complete remission after first-line chemotherapy.

Patients with histologically confirmed CD20$^+$ follicular NHL (stage III or IV) were included in the study. Within 2 weeks before inclusion, patients were required to have acceptable hematologic status (absolute neutrophil count $\geq$1500 cells/mm$^3$ and platelets $\geq$150,000 cells/mm$^3$), acceptable renal function (creatinine $\leq$2.5 $\times$ ULN [upper limit of normal]) and liver function (bilirubin $\leq$1.5 $\times$ ULN and ALAT $\leq$2.5 $\times$ ULN), and a bone marrow involvement (assessed by a bone marrow biopsy) less than 25%. Any prior chemotherapy had to have been completed no less than 6 weeks and no more than 12 weeks before $^{90}$Y-ibritumomab tiuxetan treatment. This study was conducted in accordance with the Declaration of Helsinki and approved by French authorities (Ethics Committee of Angers University Hospital, Angers, France). A written, informed consent was obtained from all patients.

On day 0 (D0), patients received 250 mg/m$^2$ rituximab to optimize the biodistribution of the radiolabeled antibody. No more than 4 hours later, an intraveinous (i.v.) injection of $^{111}$In-ibritumomab tiuxetan (185 MBq) was performed for dosimetry. One (1) week later, patients received a second infusion of rituximab (250 mg/m$^2$), followed by a therapeutic administration of 15 MBq/kg (with a maximum activity of 1.2 GBq) $^{90}$Y-ibritumomab tiuxetan (mean activity: 910 MBq, range: [844 MBq–1000 MBq]).

**CT Scans**

CT scans of both the Liqui-Phil phantom and the study patients were acquired on a Light-Speed RT scanner (General Electric Medical Systems, Chalfont St. Gilles, UK). The acquisition parameters were 140 kV, 240 mA, a slice thickness of 3.75 mm, and a matrix size of 512 $\times$ 512. The phantom inserts were filled with a contrast medium (Iopamiron 300; Schering AG) so that they could be visualized and segmented on the CT images. The remainder volume within the phantom was filled with water. The pixel size was 0.84 $\times$ 0.84 mm. Patient CT scans were performed within 1 week before or after the $^{111}$In-ibritumomab tiuxetan injection. During the CT acquisition, the patient arms were maintained along the sides of the body in the same position as during SPECT imaging. Depending on the patient girth, the pixel size varied from 0.7 $\times$ 0.7 mm to 0.84 $\times$ 0.84 mm.

**Planar and SPECT Acquisitions**

Static 2D WB and 3D SPECT acquisitions were performed on a DST-XLi double-headed gamma-camera (General Electric Medical Systems) (3"8 NaI(Tl) crystal, field of view = 540 $\times$ 400 mm) equipped with medium-energy high-resolution (MEHR) collimators.

**Table 1.** Volume and Activity in the Different Inserts of the Liqui-Phil™ Abdominal Phantom

|  | Liver | Spleen | Left kidney | Right kidney | Large sphere | Small sphere | Background |
|---|---|---|---|---|---|---|---|
| Volume (mL) | 1594 | 170 | 116 | 144 | 33.5 | 4.2 | 9050 |
| Activity (MBq) | 44.0 | 7.4 | 7.0 | 7.0 | 4.1 | 0.74 | 42.0 |

*Note.* The Liqui-Phil abdominal phantom was obtained from the Phantom Laboratory (New York, NY).

*Phantom*

Two planar acquisitions (anterior and posterior) were acquired during 230 seconds, including all events detected in any of the two 20% energy windows centered on 171 and 245 keV (matrix size = 512 × 512, pixel size = 1.13 × 1.13 mm). For the SPECT acquisition, 128 projections (20 seconds/proj, matrix size = 128 × 128, pixel size = 4.52 × 4.52 mm) were acquired over 360 degrees (radius of rotation = 34 cm) in the two 20% energy windows centered on 171 and 245 keV and in three scatter windows, 6 keV wide each: ([150 keV − 156 keV], [186 keV − 192 keV], [218 keV − 224 keV]).

*Patients*

WB and SPECT acquisitions were obtained at five time points (between 1 and 2 hours, between 3 and 4 hours and 1, 4, and 6 days) after the $^{111}$In-ibritumomab tiuxetan injection, except for 2 patients, for whom only 4 SPECT acquisitions were performed 2 hours and 1, 4, and 6 days postinjection. For the WB scans, anterior and posterior images were acquired corresponding to all events detected in one of the two 20% energy windows centered on 171 and 245 keV (matrix size = 512 × 2048, pixel size = 1.13 × 1.13 mm). The scanning speed was 14 cm/minutes for the first three time points and 10 cm/minutes for the last two time points. For the SPECT scans, 128 projections were acquired over 360 degrees (matrix size = 128 × 128, pixel size = 4.52 × 4.52 mm) with the same energy windows as for the SPECT acquisitions of the phantom. The acquisition duration was 20 seconds/proj for the first three time points and 30 seconds/proj for the last two time points. For a given patient, the radius of rotation of the detection heads was always the same, on average of 308 ± 16.7 mm for the 6 patients.

*Background activity measurements*

Seven (7) SPECT acquisitions of background activity were performed, 1 per patient and 1 for the phantom experiment. Acquisition parameters were the same as those used for the phantom and patient acquisitions, except for the number and duration of projections, which were, respectively, 64 and 10 seconds/proj.

*Calibration vial*

A calibration object consisting in a cylindrical vial (inner diameter of 2.7 cm, length of 11.5 cm,

volume of 57 mL) filled with 34 kBq/mL of $^{111}$In was used for the SPECT activity measurement. A SPECT acquisition of the vial alone was performed for the patients and the phantom with the same acquisition parameters as those used with the patients or the phantom.

**Activity Quantification**

*2D protocol*

*Phantom.* Regions of interest ($ROI_{WB}$) were manually drawn on anterior and posterior images around the liver, spleen, kidneys, and phantom inserts. A subtraction of surrounding activity estimated in a manually drawn ROI in the neighbourhood of the spheres and the kidneys was performed for the two sets of inserts. Activity in all regions was estimated using the geometric mean (GM) of anterior and posterior $ROI_{WB}$ counts (after a correction for background activity for the spheres and kidneys). A calibration factor was obtained by dividing the total activity introduced in the phantom (accounting for radioactive decay at the time of acquisition) by the result of the geometric mean of the total number of counts in the anterior and posterior acquisitions. For each insert, activity in the $ROI_{WB}$ was estimated by multiplying the measured value in the ROI by this calibration factor.

*Patients.* For the patients, the $ROI_{WB}$ were drawn on the images corresponding to the time point for which the contrast between specific and nonspecific activity was visually the highest. For each patient, $ROI_{WB}$ corresponding to the liver, the spleen, and the two kidneys were drawn on the anterior and posterior views. $ROI_{WB}$ were then manually registered on the images acquired at the other time points. A subtraction of surrounding activity was performed for the kidneys. Activity in these regions was estimated from the GM of the anterior and posterior $ROI_{WB}$ counts. A patient-specific calibration factor was obtained by dividing the injected activity by the result of the GM of the total number of counts in the first anterior and posterior acquisitions, before the first urination. For each patient, activity in the $ROI_{WB}$ was estimated by multiplying the measured value in the ROI at any time point by this calibration factor.

*3D protocol*

Patient and phantom SPECT acquisitions were systematically corrected for background activity by subtracting the corresponding background

noise projections from the projections. The two sets of projections recorded in the 20% windows centered on the ^{111}In photopeaks (171 and 245 keV) were corrected for scatter, using the triple energy window method[14]: The 171 keV photopeak window was corrected by using the [150 keV − 156 keV] and [186 keV − 192 keV] windows as scatter windows, whereas the 245-keV photopeak window was corrected by using the [218 keV − 224 keV] scatter window (no upper scatter window was used). The two sets of corrected projections were then summed and called summed projections thereafter.

Attenuation was modeled in the ordered-subset expectation maximization algorithm (OSEM; 8 iterations and 6 subsets).[15] A uniform attenuation correction was used for the phantom experiment, whereas a nonuniform attenuation map was used for the patients. The attenuation maps were obtained by scaling the attenuation map from the CT energy to 171 and 245 keV separately.[16] These scaled CT maps were then registered on reconstructed SPECT data, using an auto-correlation method.[17] An effective attenuation map, appropriate for correcting the summed projections, was obtained as a weighted sum of the 171 and 245 keV attenuation maps (weights of 0.49 and 0.51, respectively) to account for the respective contribution of the 171 and 245 keV in the emission spectrum. After reconstruction, the partial volume effect (PVE) was compensated for by using recovery coefficients.[18] The coefficients were calculated for 3D volumes of interest ($VOI_{SPECT}$), manually drawn on CT around the organs of interest (e.g., the liver, spleen, kidneys, and the two spheres), by convolving the binary image of each VOI with a 3D-Gaussian with a full width at half maximum (FWHM) equal to the spatial resolution in the reconstructed images. The FWHM was estimated by using the images of a cylindrical phantom, including five spheres reconstructed by using the very same protocol as the anthropomorphic phantom and patient images, and was found to be 18.1 mm.

Insert and organ activities were estimated by multiplying the number of counts measured in each $VOI_{SPECT}$ by the calibration factor derived from the vial acquisitions. This calibration factor was defined as equal to the ratio of the true activity in the calibration vial and the total number of counts measured on the reconstructed SPECT images of the vial. The difference in detection efficiency for the 171- and 245-keV photons was accounted for through the calibration factor only.

Additional experiments in which activity estimates were obtained from the two energy windows separately, with one specific calibration factor for each energy window (hence, satisfactorily accounting for the difference in detection efficiency as a function of energy), yielded results that were very close to those obtained when summing the events detected in the two energy windows and using a single calibration factor. This suggests that although approximate, this calibration approach did not introduce large errors in activity estimates. Because of the small size of the vial, no correction was applied during the SPECT reconstruction of the calibration object.

## Organ Mass Estimates

Organ mass estimates were needed for calculating the dose in patients. For the patient data under the 2D protocol, organ masses ($m_{MIRD}$) corresponding to those available in the software MIRDOSE 3 were considered.[19] For the patient data under the 3D protocol, the liver, the spleen, and the 2 kidneys were manually drawn on the CT patient data. The corresponding organ masses ($m_{CT}$) were calculated by considering a soft-tissue density of 1.05 g/cm$^3$.[20]

## Absorbed Dose Estimate

The radiation-absorbed dose calculations were performed by using ZevMIRD software (RBA, San Diego, CA), which is based on the MIRDOSE 3 computation.[19] This software can calculate the organ residence time for $^{90}$Y, based on the $^{111}$In-ibritumomab tiuxetan activity values.

The data points representing the fraction of injected activity (FIA) in an organ at different time points were calculated by taking into account the difference of decay constant between $^{111}$In and $^{90}$Y. $FIA_{WB}$ and $FIA_{SPECT}$ were fitted to monoexponential time-activity curves (TAC).[21] After curve fitting and integration, the cumulated activity and residence time were calculated for each organ and acquisition protocol (2D and 3D).

The radiation-absorbed doses were calculated when given the residence times of the target organs. For patient-specific 3D dosimetry, the radiation-absorbed dose was corrected for organ mass by the ratio of ($m_{MIRD}$) to the actual organ mass ($m_{CT}$) of the patient. When using the 2D protocol, doses were calculated without and with accounting for CT-derived organ masses.

**Table 2.** Relative Difference Between the Real Volume of the Insert and the Measured Volume on Computed Tomography Scan for the Liqui-Phil™ Abdominal Phantom

|  | Liver | Spleen | Left kidney | Right kidney | Large sphere | Small sphere |
|---|---|---|---|---|---|---|
| Real volume (mL) | 1594 | 170 | 116 | 144 | 33.5 | 4.2 |
| Measured volume (mL) | 1592 | 174 | 119 | 146 | 34.0 | 4.4 |
| Error[a] (%) | −0.1 | 2.4 | 2.6 | 1.4 | 1.4 | 5.8 |

*Note*. The Liqui-Phil abdominal phantom was obtained from the Phantom Laboratory (New York, NY).
[a]Error = [(measured volume − real volume)/real volume]*100.

## RESULTS

In the phantom experiment, the relative difference between the volume measured from the CT of the inserts and the real volume of the inserts (100*([measured volume − true volume]/true volume) was less than 2.6%, except for the smallest sphere of 4.4 mL, for which the relative difference reached 5.8% (Table 2).

Our patients' data showed a large variability in organ masses (Table 3). In most cases, the CT-derived organ mass was higher than the standardized organ mass, leading to a radiation-absorbed dose overestimation when using the anthropomorphic model.[19] The mean differences between the CT-derived patient organ mass and the MIRD anthropomorphic model (100*[CT-derived mass − MIRD mass]/MIRD mass) was 11%, 98%, and 16% for liver, spleen, and kidneys in the female patients and −10%, 57%, and 16% for liver, spleen, and kidneys in the male patients.

Using the phantom data, the activity values were, overall, more accurately estimated when using the SPECT protocol, including corrections (Table 4). The activity in the smallest sphere was poorly estimated with both the 2D and 3D protocols. Excluding this sphere, the error in activity estimates (100*[estimated activity − true activity]/true activity) was between −6% and −23% when using quantitative SPECT and between −86% and 18% when using the WB protocol. The activity differences between SPECT and WB estimates (100*(SPECT activity estimate − WB activity estimate)/WB activity estimate) were −14% for liver, −7% for spleen, −23% for the right kidney, and +28% for the left kidney.

In the patients, the mean percent differences (±1 standard deviation) between SPECT and WB

**Table 3.** Actual Organ Mass Defined on Computed Tomography Scans, Mean Value by Gender and the Corresponding Mass Used with an Anthropomorphic Model[19]

|  |  | Organ mass (g) | | |
|---|---|---|---|---|
|  |  | Liver | Spleen | Kidney |
| Females | 1 | 1240 | 163 | 293 |
|  | 2 | 1581 | 418 | 299 |
|  | 3 | 1702 | 279 | 293 |
|  | 5 | 1715 | 110 | 263 |
|  | Mean ± standard deviation | 1560 ± 192 | 243 ± 118 | 287 ± 14 |
|  | MIRD anthropomorphic phantom | 1400 | 123 | 248 |
| Males | 4 | 1909 | 416 | 319 |
|  | 6 | 1537 | 157 | 372 |
|  | Mean | 1723 ± 186 | 287 ± 130 | 346 ± 27 |
|  | MIRD anthropomorphic phantom | 1910 | 183 | 299 |

Superscripted "19" refers to Reference 19.
MIRD, Medical Internal Radiation Dose.

activity estimates (100*[SPECT activity estimate − WB activity estimate]/WB activity estimate) were −32% ± 20%, −59% ± 27% and −38% ± 41% (n = 28 activity measurements) for liver, spleen, and kidneys, respectively (Table 5).

Examples of TACs measured in a patient for liver, spleen, and kidneys are shown in Figure 1. The semilogarithmic representation of FIA shows an appropriate linear fit for both WB and SPECT data, suggesting that the monoexponential model is relevant.[21] The correlation coefficients ($R^2$) of the linear fits averaged over the 6 patients and 3 organs (liver, spleen, and kidneys) were 0.989 ± 0.009 and 0.986 ± 0.012 for WB and SPECT protocols, respectively, with no significant difference between these two values ($p = 0.42$).

Tables 6 and 7 present the mean and range of the radiation-absorbed dose to liver, spleen, and kidneys estimated from the 2D and 3D protocol, respectively, with and without organ-mass scaling. On average, the absorbed doses estimated when using the 3D protocol were smaller than those estimated when using the 2D protocol. The mean percent difference between the 3D and 2D estimates without organ correction (100*[3D dose − 2D dose]/2D dose) was −29% ± 26% for liver (range, −61% to +9%), −73% ± 20% for spleen (range, −97% to −52%), and −33% ± 53% for kidneys (range, −89% to +43%).

## DISCUSSION

In relapsed or refractory NHL patients treated by ^{90}Y-ibritumomab tiuxetan with a therapeutic administered activity of 15 MBq/kg (maximum 1.2 GBq), Wiseman et al. found that dose estimates did not correlate with bone-marrow radiotoxicity.[7] This result was also reported by Erwin et al.[22] Patients with adequate bone-marrow reserve and <25% bone-marrow involvement are treated with an amount of ^{90}Y-ibritumomab tiuxetan activity determined from body weight only. Most clinical radionuclide therapy studies have shown an absent, or rather weak, relationship between radiation-absorbed dose and radiotoxicity to normal tissues.[11–13] Recently, several researchers have proposed to improve the efficacy of radionuclide therapy by bone-marrow reconstitution,[23] fractionated therapy,[24] or pretargeted therapy.[25] Larger amounts of activity can thus be administered before the critical organ tolerance is reached. For these applications, 3D dosimetry protocol might help to understand the correlation between the absorbed dose and clinical outcome of the treatment.[23]

Comparing 2D WB and 3D SPECT protocols for dose estimates, our results suggest that accounting for patient-specific organ masses and estimating activity values from 3D SPECT data had a significant impact on dose estimates. The large differences between (1) reference (anthropomorphic phantoms) and actual organ masses and (2) activity estimates from WB and SPECT protocols led to large differences in absorbed-dose estimates between a 2D and 3D model. Organ masses and activity largely contribute to the final dose estimates, (i.e., dose proportional to the cumulated activity and inversely proportional to the mass), and the accuracy with which they can be estimated is to be considered to improve the dosimetry assessment. For our patients, both sources of error tend to overestimate the organ dose.
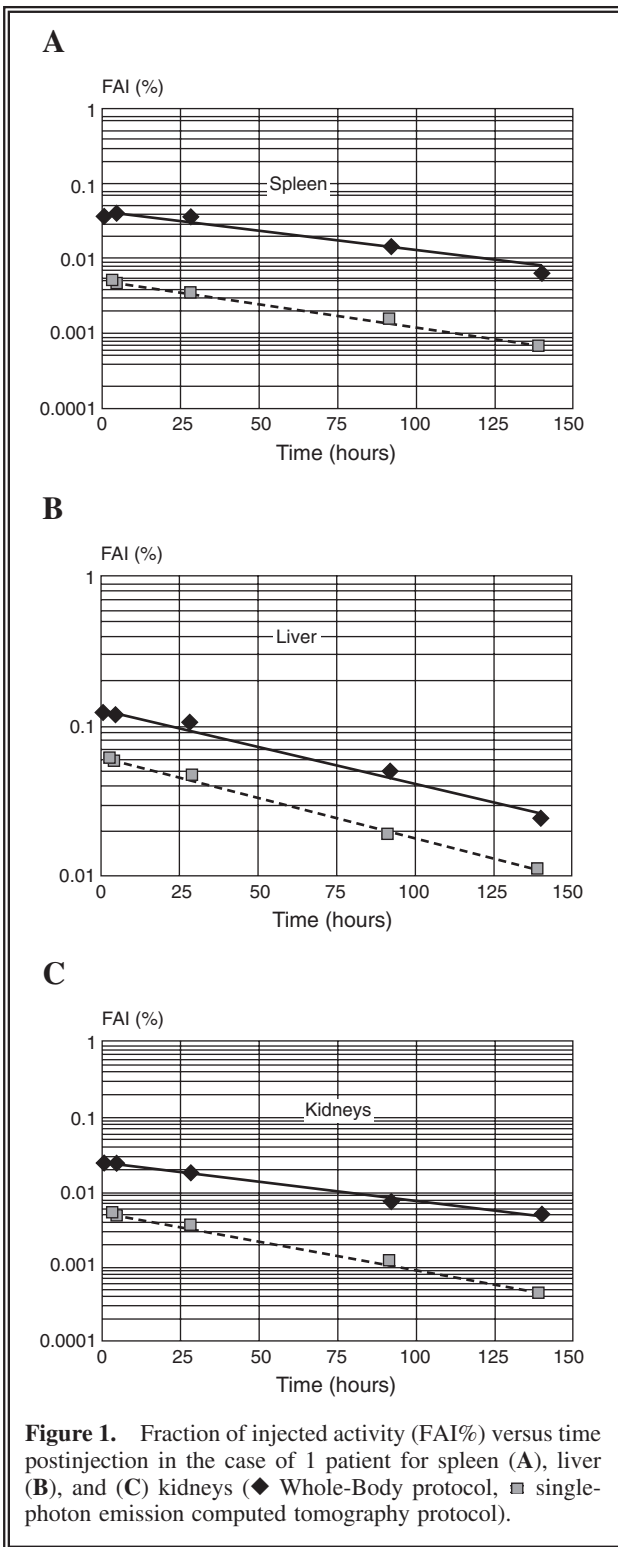
Looking first at the impact of mass estimates on dose estimates, our patients' data showed large

**Table 5.** Mean and Range of Relative Activity Differences Between SPECT and WB Imaging (n = 28 Activity Measurements) [(SPECT Activity Estimate − WB Activity Estimate)/WB Activity Estimate]*100

| Organ | Mean | Range |
|---|---|---|
| Liver | −32 | [−71; −4] |
| Spleen | −59 | [−92; −12] |
| Kidney | −38 | [−93; +46] |

SPECT, single-photon emission computed tomography; WB, whole body.

**Table 4.** Relative Difference Between [111]In Activity Set in the Phantom and Activity Measured from WB and SPECT Imaging for the Liqui-Phil™ Abdominal Phantom [(Estimated Activity − Real Activity)/Real Activity]*100

| Insert | WB | SPECT |
|---|---|---|
| Liver | 10 | −6 |
| Spleen | −3 | −10 |
| Left kidney | −40 | −23 |
| Right kidney | 18 | −9 |
| Sphere (40) | −86 | −9 |
| Sphere (20) | −80 | −43 |

The Liqui-Phil abdominal phantom was obtained from The Phantom Laboratory (New York, NY).

WB, whole body; SPECT, single-photon emission computed tomography.

**Figure 1.** Fraction of injected activity (FAI%) versus time postinjection in the case of 1 patient for spleen (**A**), liver (**B**), and (**C**) kidneys (◆ Whole-Body protocol, ▦ single-photon emission computed tomography protocol).

variability in organ masses (Table 3), questioning the relevance of using fixed organ masses for dose calculations, in particular in hematologic pathologies were most organs (e.g., spleen and

liver) may have large hypertrophy. This is in agreement with previous reports.[10,11] For instance, Rajendran et al.[10] found mean and range (in parenthesis) CT volumes of 1782 mL (range, 662–3,420) to liver, 316 mL (range, 50–639) to spleen, and 381 mL (range, 230–661) to kidneys, in 84 patients treated by ^{131}I-tositumab RIT for NHL, without differentiating the gender. The CT scan is a well-established method for estimating organ volumes.[26,27] In the phantom experiment, we found a good agreement between the volume of the phantom inserts and the volumes as estimated from the CT scan. Large differences between the patient organ mass estimated from the CT and the organ mass of the anthropomorphic model were observed[19] (Table 2), especially in the spleen affected by the disease. Since the absorbed dose to an organ is inversely proportional to the organ mass, an adjustment of the actual organ volume derived from CT imaging is a prerequisite for a reliable dosimetry estimate.

Organ masses based on CT volumetry can also be used in a 2D dosimetry protocol.[7] However, using a 3D protocol also makes it possible to get precise data for attenuation and partial volume effect corrections of SPECT data. In addition, SPECT/CT protocols improve the prediction of myelotoxicity from bone-marrow dosimetry in the case of RIT,[28,29] involving a CT scan in the dosimetry protocol. The CT scan should, therefore, be of great benefit and will be facilitated in the future owing to SPECT/CT machines that become widely available. For most radionuclides, the $\beta^-$ self-dose in a source organ is the main contribution to the total organ dose. So, a simple organ mass correction is accurate for pure $\beta$-emitters, such as [90]Y.[11] However, this would not be sufficient for $\gamma$-emitting radionuclides because of the penetrating character of the emission. Some software, such as OLINDA,[30] can account for patient-specific organ masses for the photon self-dose calculation but not for the photon cross-dose calculation.

Considering organ-activity estimates, accurate quantification of ^{111}In images is a prerequisite to derive accurate activity estimates in various organs or tumors, which are then used to calculate accurate doses for a radiopharmaceutical labeled with [90]Y. A phantom study was performed to assess the accuracy of activity quantification when using whole-body and SPECT data. The whole-body activity measurements were performed as suggested under the guidance of the MIRD Committee for a 2D protocol.[5] In this approach, the

**Table 6.** Dosimetry Estimate Results Without Organ Mass Scaling After Administration of a Therapeutic Activity of ^{90}Y-Ibritumomab Tiuxetan − 15 MBq/kg with a Maximum Activity of 1.2 GBq (n = 6)

| Organs | Absorbed dose (Gy) 2D protocol without mass correction | | Absorbed dose (Gy) 3D protocol without mass correction | |
|---|---|---|---|---|
| | Mean | Range | Mean | Range |
| Liver | 3.1 | 2.3–3.8 | 2.2 | 1.8–2.8 |
| Speen | 6.9 | 3.7–9.9 | 2.1 | 0.84–4.2 |
| Kidneys | 2.2 | 1.35–3.3 | 1.6 | 0.31–4.2 |

2D, 3D, two- and three dimensional.

organ activity is estimated from the geometric mean of ROI counts measured in the anterior and posterior views. To improve the accuracy of activity estimates, several more or less sophisticated correction methods were also proposed by the MIRD Committee,[5] but no precise protocol involving such corrections has been set as a standard protocol. In our study, we considered the 2D protocol described by Wiseman et al. to determine the cumulated activity and the residence time, including corrections for activity surrounding small structures (i.e., kidneys and spheres) and for attenuation.[7] Attenuation is indirectly compensated for by using the number of counts recorded in the first WB scan, before urination, to define the calibration factor. Indeed, this calibration factor, by relating the number of detected counts to the actual activity in the patient before voiding, accounts for the overall photon attenuation produced by the patient. Multiplying subsequent measurements by this calibration factor, therefore, roughly compensates for attenuation, although this is, by no means, a locally accurate attenuation compensation. More accurate 2D pro-

tocols could have been used, for instance, including a scatter correction and a more sophisticated attenuation correction, but in the absence of a "standard" 2D protocol, any choice can be made, and we chose to consider the activity measurement protocol published in the summary of product characteristics of ZEVALIN. With this methodology, Wiseman et al. estimated the median and the range of the absorbed dose to spleen (7.42 Gy [0.76–24.5]), to liver (4.50 Gy [1.22–18.6]), and to kidney (0.23 Gy [0–0.76]) in 129 patients treated by ^{90}Y ibritumomab tiuxetan with a therapeutic administered activity of 15 MBq/kg (maximum, 1.2 GBq). Our dosimetry estimates with the 2D protocol are in the same range of value, except in the kidneys.[7] Delineation of kidney on planar images, being extremely difficult owing to the low uptake of the radiopharmaceutical, large errors in this organ can be expected when using 2D protocols.

The limits of 2D activity estimates were demonstrated by using our phantom experiments, with a relative difference between estimated activity and real ^{111}In activity ranges from −86%

**Table 7.** Dosimetry Estimate Results With Organ Mass Scaling After Administration of a Therapeutic Activity of ^{90}Y-Ibritumomab Tiuxetan − 15 MBq/kg with a Maximum Activity of 1.2 GBq (n = 6)

| Organs | Absorbed dose (Gy) 2D protocol with mass correction | | Absorbed dose (Gy) 3D protocol with mass correction | |
|---|---|---|---|---|
| | Mean | Range | Mean | Range |
| Liver | 3.0 | 2.5–4.3 | 2.1 | 1.3–2.6 |
| Speen | 4.2 | 2.9–6.1 | 1.5 | 0.30–2.6 |
| Kidneys | 1.9 | 1.2–2.7 | 1.4 | 0.26–3.0 |

2D, 3D, two- and three dimensional.

to +18%. This wide extent is owing to the overlapping of the structures, scatter, and partial volume effect, as all these effects are not compensated for properly in the 2D protocol. In particular, activity estimates are very different for right and left kidneys, because of the overlap of the right kidney with the liver. Even if several methods were proposed in the literature to improve the accuracy of activity estimates in planar imaging,[5] it is now well accepted that accurate quantification requires SPECT imaging, involving a number of correction, mostly for photon attenuation, scatter and partial volume effect, and that using these corrections, reasonable quantitative accuracy can be achieved.[23,31,32] Our study involving the Liqui-Phil phantom confirmed that the greatest accuracy in terms of activity estimate was obtained when using the quantitative SPECT protocol (Table 4), except in the smallest sphere. The large quantitative error still affecting the activity estimate in the smallest sphere can be explained by the size of this sphere, of the order of the spatial resolution in the reconstructed images. Others have previously reported the difficulty in properly estimating activity in small structures, even with appropriate imaging corrections.[23,31] It should be underlined that corrections for photon attenuation as well as scatter and partial volume effect are essential to obtain accurate activity estimates in most structures in SPECT. When considering SPECT without any correction for scatter, attenuation, and partial volume effect, all insert activity values were underestimated by more than 60%.

For patients, there was no way to objectively determine the accuracy of activity estimates in organs from WB and SPECT scans. We, therefore, compared the percent differences between SPECT and WB activity estimates observed in patients with those observed in the phantom. In the phantom, the percent differences between SPECT and WB activity (with respect to WB estimates) were −14%, −7%, +28%, and −23% for the liver, spleen, right kidney, and left kidney, respectively. These values fall in the range of those observed in patients (Table 5), except in the spleen, where the differences observed in patients tended to be slightly more pronounced than in the phantom. However, these comparisons together with the comparative errors of activity estimates in the different compartments of the phantom shown in Table 4 suggest that the 3D SPECT protocol yields more accurate activity estimates in the different organs than the 2D pro-

tocol we considered, and that the amplitude of the difference between activity estimates obtained with the two protocols is far from being negligible. These results show that WB scintigraphy should not be used for targeted therapy treatment planning. Anthropomorphic phantoms must be restricted to radiation protection. SPECT-based dosimetry, although more reliable, can be biased. It should then be used with caution. SPECT acquisition and reconstruction protocols must be thoroughly evaluated to assess the accuracy of local activity estimates from SPECT images.

A recent study demonstrated the importance of using multiple 3D image sets to obtain cumulated activity images for 3D dosimetry,[33] whereas several researchers have proposed to define time-activity curves from series of planar imaging adjusted by a single quantitative SPECT.[23,34] This approach assumes a constant ratio between the absolute activity level determined by conjugate views and SPECT imaging for all scans acquired over time in a given patient. For our patients, by adjusting WB time-activity curves by the corresponding quantitative SPECT obtained at time day 4, the mean percent difference between absorbed doses estimated when using a full 3D protocol and a planar protocol adjusted by a single SPECT acquisition was −0.3% ± 6.3% for liver (range, −8.3% to +6.3%), −2.9% ± 6.1% for spleen (range, −13.5% to +3.4%), and 5.3% ± 23.6% for kidneys (range, −17.9% to +50.0%). Because differences up to 50% were observed in the kidneys, these results suggest that it might be worth using a full 3D approach rather than combining the 2D and 3D approaches, especially as the development of SPECT/CT machines now makes it possible to perform SPECT and CT acquisitions relatively quickly. Nevertheless, the use of a single quantitative SPECT combined with a series of WB scans provides a substantially improved absorbed-dose estimation, compared with conjugate-view scans alone.[34]

## CONCLUSIONS

Considering 6 patients, we have compared dose estimates in liver, spleen, and kidneys as obtained from a 3D SPECT imaging protocol and personalized organ mass estimates with those obtained using a 2D planar imaging protocol and fixed reference organ mass. The 2D activity measurement protocol used was similar to the one published in

the summary of product characteristics of ZE-VALIN. We found large discrepancies between dose estimates from the two protocols, and the amplitude of the discrepancy was organ- and patient dependent. Overall, absorbed doses tended to be larger when using the 2D protocol than when using the 3D protocol. We conclude that the estimation of absorbed doses from SPECT activity measurements and personalized organ mass estimates contribute to a more accurate assessment of the dose distribution in patients.

## REFERENCES

1. Witzig TE, Gordon LI, Cabanillas F, et al. Randomized, controlled trial of yttrium-90-labeled ibritumomab tiuxetan radioimmunotherapy versus rituximab immunotherapy for patients with relapsed or refractory low-grade, follicular, or transformed B-cell non-Hodgkin's lymphoma. *J Clin Oncol* 2002;20:2453.

2. Gansow OA. Newer approaches to the radiolabeling of monoclonal antibodies by use of metal chelates. *Int J Rad Appl Instrum B* 1991;18:369.

3. Chinn PC, Leonard JE, Rosenberg J, et al. Preclinical evaluation of $^{90}$Y-labeled anti-CD20 monoclonal antibody for treatment of non-Hodgkin's lymphoma. *Int J Oncol* 1999;15:1017.

4. Vallabhajosula S, Goldsmith SJ, Hamacher KA, et al. Prediction of myelotoxicity based on bone marrow radiation-absorbed dose: Radioimmunotherapy studies using $^{90}$Y- and $^{177}$Lu-labeled J591 antibodies specific for prostate-specific membrane antigen. *J Nucl Med* 2005; 46:850.

5. Siegel JA, Thomas SR, Stubbs JB, et al. MIRD pamphlet no. 16: Techniques for quantitative radiopharmaceutical biodistribution data acquisition and analysis for use in human radiation dose estimates. *J Nucl Med* 1999;40:37S.

6. Loevinger R, Budinger TF, Watson EE. *MIRD Primer for Absorbed Dose Calculations,* rev. ed. New York: Society of Nuclear Medicine, 1991.

7. Wiseman GA, Kornmehl E, Leigh B, et al. Radiation dosimetry results and safety correlations from $^{90}$Y-ibritumomab tiuxetan radioimmunotherapy for relapsed or refractory non-Hodgkin's lymphoma: Combined data from 4 clinical trials. *J Nucl Med* 2003;44:465.

8. Jönsson L, Ljungberg M, Strand SE. Evaluation of accuracy in activity calculations for the conjugate view method from Monte Carlo simulated scintillation camera images using experimental data in an anthropomorphic phantom. *J Nucl Med* 2005;46:1679.

9. Clairand I, Bouchet LG, Ricard M, et al. Improvement of internal dose calculations using mathematical models of different adult heights. *Phys Med Biol* 2000; 45:2771.

10. Rajendran JG, Fisher DR, Gopal AK, et al. High-dose (131)I-tositumomab (anti-CD20) radioimmunotherapy for non-Hodgkin's lymphoma: Adjusting radiation absorbed dose to actual organ volumes. *J Nucl Med* 2004; 45:1059.

11. DeNardo GL, DeNardo SJ, Shen S, et al. Factors affecting $^{131}$I-Lym-1 pharmacokinetics and radiation dosimetry in patients with non-Hodgkin's lymphoma and chronic lymphocytic leukemia. *J Nucl Med* 1999;40:1317.

12. Sgouros G, Squeri S, Ballangrud AM, et al. Patient-specific, 3-dimensional dosimetry in non-Hodgkin's lymphoma patients treated with $^{131}$I-anti-B1 antibody: Assessment of tumor dose-response. *J Nucl Med* 2003; 44:260.

13. Koral KF, Dewaraja Y, Li J, et al. Update on hybrid conjugate-view SPECT tumor dosimetry and response in $^{131}$I-tositumomab therapy of previously untreated lymphoma patients. *J Nucl Med* 2003;44:457.

14. Ogawa K, Harata Y, Ichihara T, et al. A practical method for position-dependent Compton-scatter correction in single photon emission CT. *IEEE Trans Nucl Sci* 1991;10:408.

15. Hudson HM, Larkin RS. Accelerated image reconstruction using ordered subsets of projection data. *IEEE Trans Med Imaging* 1994;13:601.

16. Burger C, Goerres G, Schoenes S, et al. PET attenuation coefficients from CT images: Experimental evaluation of the transformation of CT into PET 511-keV attenuation coefficients. *Eur J Nucl Med Mol Imaging* 2002;29:922.

17. Junck L, Moen JG, Hutchins GD, et al. Correlation methods for the centering, rotation, and alignment of functional brain images. *J Nucl Med* 1990;31:1220.

18. Muzic RF, Jr, Chen CH, Nelson AD. A method to correct for scatter, spillover, and partial volume effects in region of interest analysis in PET. *IEEE Trans Med Imaging* 1998;17:202.

19. Stabin MG. MIRDOSE: Personal computer software for internal dose assessment in nuclear medicine. *J Nucl Med* 1996;37:538.

20. International Commission on Radiation Units and Measurements. *Photon, Electron, Proton and Neutron Interaction Data for Body Tissues*, ICRU Report 46. Oxford: Oxford University Press, 1992.

21. Erwin WD, Groch MW. Quantitative radioimmunoimaging for radioimmunotherapy treatment planning: Effect of reduction in data sampling on dosimetric estimates. *Cancer Biother Radiopharm* 2002;17:699.

22. Erwin WD, Spies SM, Kelly ME, et al. Correlation of marrow dose estimates based on serial pretreatment radiopharmaceutical imaging and blood data with actual marrow toxicity in anti-CD20 yttrium-90 monoclonal antibody radioimmunotherapy of non-Hodgkin's B-cell lymphoma. *Nucl Med Commun* 2001;22:247.

23. Dewaraja YK, Wilderman SJ, Ljungberg M, et al. Accurate dosimetry in $^{131}$I radionuclide therapy using patient-specific, 3-dimensional methods for SPECT reconstruction and absorbed dose calculation. *J Nucl Med* 2005;46:840.

24. DeNardo GL, DeNardo SJ, Goldstein DS, et al. Maximum-tolerated dose, toxicity, and efficacy of (131)I-Lym-1 antibody for fractionated radioimmunotherapy of non-Hodgkin's lymphoma. *J Clin Oncol* 1998;16:3246.

25. Weiden PL, Breitz HB. Pretargeted radioimmunotherapy (PRIT) for treatment of non-Hodgkin's lymphoma (NHL). *Crit Rev Oncol Hematol* 2001;40:37.

26. Schiano TD, Bodian C, Schwartz ME, et al. Accuracy and significance of computed tomographic scan assessment of hepatic volume in patients undergoing liver transplantation. *Transplantation* 2000;69:545.

27. Heymsfield SB, Fulenwider T, Nordlinger B, et al. Accurate measurement of liver, kidney, and spleen volume and mass by computerized axial tomography. *Ann Intern Med* 1979;90:185.

28. Shen S, Meredith RF, Duan J, et al. Improved prediction of myelotoxicity unsing a patient-specific imaging dose estimate for non-marrow-targeting $^{90}$Y-antibody therapy. *J Nucl Med* 2002;43:1245.

29. Boucek JA, Turner JH. Validation of prospective whole-body bone marrow dosimetry by SPECT/CT multi-modality imaging in $^{131}$I-anti-CD20 rituximb radioimmunotherapy of non-Hodgkin's lymphoma. *Eur J Nucl Med Mol Imaging* 2005;32:458.

30. Stabin MG, Siegel JF. Physical models and dose factors for use in internal dose assessment. *Health Phys* 2003;85:294.

31. Soret M, Koulibaly PM, Darcourt J, et al. Quantitative accuracy of dopaminergic neurotransmission imaging with (123)I SPECT. *J Nucl Med* 2003;44:1184.

32. He B, Du Y, Song X, et al. A Monte Carlo and physical phantom evaluation of quantitative In-111 SPECT. *Phys Med Biol* 2005;50:4169.

33. Sgouros G, Kolbert KS, Sheikh A, et al. Patient-specific dosimetry for $^{131}$I thyroid cancer therapy using $^{124}$I PET and 3-dimensional-internal dosimetry (3D-ID) software. *J Nucl Med* 2004;45:1366.

34. Frey EC, He B, Sgouros G, et al. Comparison of planar, quantitative SPECT, and combined planar-quantitative SPECT organ residence time estimation methods for targeted radionuclide therapy dosimetry [abstract]. *J Nucl Med* 2004;45(Suppl.):46P.